SCIENTIFIC REPORTS
nature research

OPEN

Oxygen-Cluster-Modified Anatase with Graphene Leads to Efficient and Recyclable Photo-Catalytic Conversion of CO_2 to CH_4 Supported by the Positron Annihilation Study

Received: 6 June 2019
Accepted: 20 August 2019
Published online: 11 September 2019

Gulzar Ahmed[1,5], Fazal Raziq[2], Muddasir Hanif[1,3], Javid Khan[4], Khurram Shahzad Munawar[5], Mingmei Wu[4], Xingzhong Cao[6] & Zhongwu Liu[1]

Anatase TiO_2 hollow nanoboxes were synthesized and combined with the graphene oxide to get nanocomposite of TiO_2/rGO (TG). Graphene oxide was used to modify the Oxygen-Clusters and bulk to surface defects. Anatase and TG composite were characterized with the positron annihilation, XPS, EPR, EIS and photocurrent response analysis. The relative affects of defects on the photocatalytic reduction (CO_2 to CH_4) were studied. The TG composites showed highest photo-catalytic activity after GO coupling (49 µmol g^{-1} h^{-1}), 28.6 times higher photocurrent yields much higher quantum efficiency (3.17%@400 nm) when compared to the TiO_2 nanoboxes. The mechanism of enhanced photo-catalytic CO_2 conversion to CH_4 elucidated through electrochemical and photo-catalytic experiments with traceable isotope containing carbon dioxide ($^{13}CO_2$). For the first time we discovered that diminishing the comparative concentration ratio of anatase from the bulk to surface defects could significantly increase the conversion of CO_2 to CH_4.

The carbon dioxide (CO_2) emission is one of the serious environmental problems, therefore its reduction and sustainable conversion to fuels by using solar energy is highly desirable[1]. Titania (TiO_2) is a chemically stable and biologically benign photo-catalyst, capable to convert harmful pollutants, particularly CO_2 reduction to fuel CH_4[2]. Beside the well-known bulk defects, the surface defects are more sensitive to the photocatalytic activities. The surface defects in a pure crystal can act as e-h trap-sites along with the adsorption sites on the other hand the bulk defects act only as charge carrier traps where e-h are more likely to recombine. Therefore, there is great scientific importance to understand both the bulk and surface defect states. This study highlights the defect density effects on the photocatalytic activities, which may lead to the innovative design of photocatalysts. The defects in TiO_2 have been experimentally studied by the scanning tunneling microscopy (STM)[3], electron paramagnetic resonance (EPR)[4], time-resolved photoluminescence spectroscopy (PL)[5] etc. These techniques allow understanding the effects of surface or subsurface defects, thereby helped to correlate the adsorption and surface reactivity.

The surface of graphene oxide consists of oxygen and hydroxyl functional groups capable to form new bonds with the TiO_2. When combined with graphene, the composite provides an effective approach to improve the photo-catalytic efficiency and light response. This occurs because graphene layers with 2D sp^2-hybridized carbon atoms (pi-bond conjugated structure) have superior electronic properties and large specific surface area that significantly enhances the photo-catalytic properties[6,7]. Compared with the other defect-probes techniques, positron

[1]School of Materials Science and Engineering, South China University of Technology, Guangzhou, 510640, P.R. China. [2]School of Physics, University of Electronic Science and Technology of China, Chengdu, 610054, P.R. China. [3]State Key Laboratory of Luminescent Materials and Devices, South China University of Technology, Guangzhou, 510640, P.R. China. [4]MOE Key Laboratory of Bioinorganic and Synthetic Chemistry, School of Chemistry and Chemical Engineering, SunYat-Sen University, Guangzhou, 510275, P.R. China. [5]University of Sargodha Sub Campus Mianwali, 42200, Punjab, Pakistan. [6]Institute of High Energy Physics, Chinese Academy of Sciences, Beijing, 100049, P.R. China. Correspondence and requests for materials should be addressed to G.A. (email: gulzar.ahmed@uos.edu.pk) or M.H. (email: muddasirhanif@yahoo.com) or Z.L. (email: zwliu@scut.edu.cn)

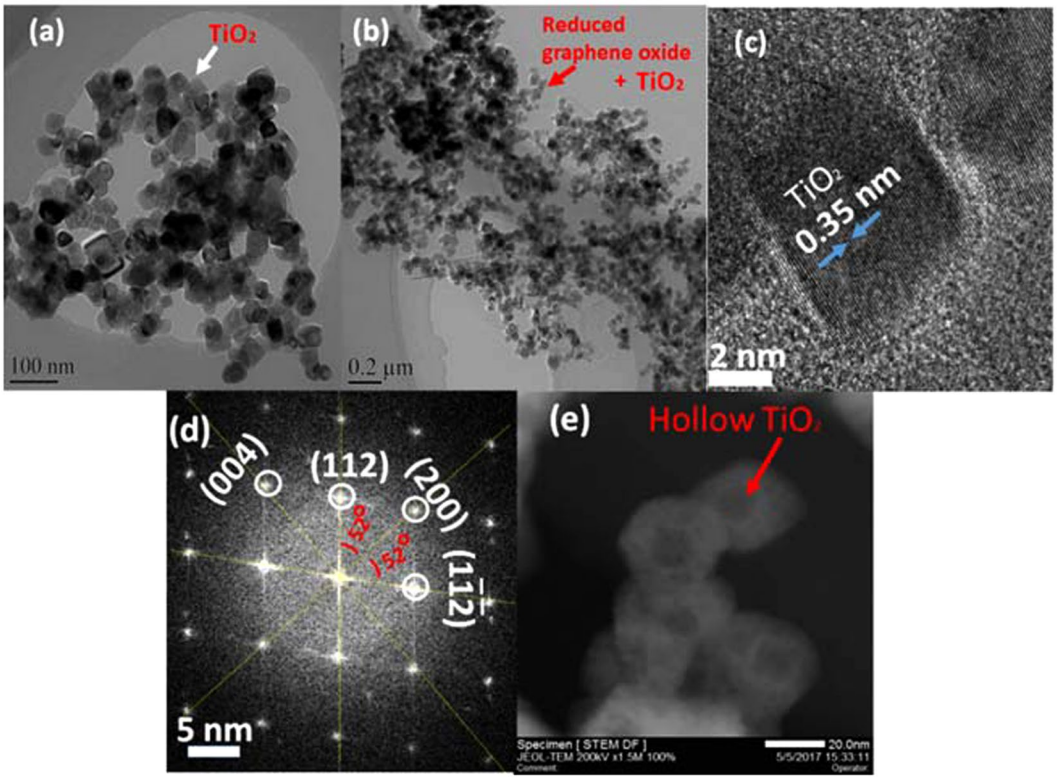

Figure 1. Characterization of TiO_2 hollow nanoboxes and TG composite. (**a**) Bright-field TEM images of the hollow TiO_2 nanoboxes. (**b**) TEM of TiO_2@rGO (TG composite). (**c**) The HRTEM shows the lattice spcing 0.35 nm (101). (**d**) corresponding SAED pattern. (**e**) STEM of hollow TiO_2.

annihilation lifetime spectroscopy (PALS) is a non-destructive technique with many advantages. For example, PALS is capable to probe not only surface but also bulk defects, sensitive to all kinds of defects particularly defects with complex structures such as open volume porousity, aggregates, voids, disclocations and grain boundaries. Therefore, PALS is a good addition to the XPS, EPR and PL techniques.

Herein, TiO_2 nano-boxes with bulk/surface defects were synthesized and characterized with the positron annihilation. We found that lowering the relative bulk to surface defects concentration ratio improved the photocatalysis efficiency. We report exceptionally enhanced photocatalytic CO_2 reduction capability of titania through defects and structural engineering, as well as magnetic titania hybrid for efficient recyclability. Simple routes were developed to synthesize the nano-crystalline anatase TiO_2 with hollow structure of nano-boxes. For the defect engineering and photocatalytic properties, nanocomposites of TiO_2/rGO (TG) and TiO_2-(Fe_3O_4@SiO_2)/rGO (TFSG) hybrids were synthesized through controlled microwave processing strategy. To improve the recyclability, TFSG samples with Fe_3O_4 magnetic nano-core and SiO_2 protecting shell were synthesized for the recovery of catalyst. Herein we discuss our findings in detail.

Results and Discussion

Structural characterization and surface composition. The XRD spectra of TiO_2, and TG composite (Supplementary Fig. 1a(i)) indicates that the samples have crystalline nature. The diffraction peaks indexed as (101), (004), (200), (105), (211), (204), (116), (220), (215) and (224) for the anatase phase matched well with the reference (JCPDS: 01-071-1166), indicating a single phase. The obtained TG sample shows TiO_2 peaks because rGO is not sensitive to the XRD (Supplementary Fig. 1a(ii))[8]. The Raman spectra of composites (Supplementary Fig. 1b) exhibit typical features of rGO with D-band at 1354 cm^{-1} and G-band at 1611 cm^{-1}. The remaining four peaks from 100–700 cm^{-1} belong to the TiO_2. When the geometric size of TiO_2 crystal approaches to nanometer range, the E_g Raman active mode blue-shifts to 150 cm^{-1} (instead of 143 cm^{-1}) for the bulk phase[9]. The other specific vibration modes at 400 cm^{-1} (B_{1g}), 523 cm^{-1} ($B_{1g+}A_{1g}$) and 643 cm^{-1} (E_g) are characteristic peaks of the anatase phase.

The C1s XPS spectra indicated the existence of chemical binding between TiO_2 and rGO (details in Supplementary information D1). Compared with the blank GO, the new peak at 285.5 eV is ascribed to the Ti-O-C bonding. Therefore there is covalent bonding between the TiO_2 and rGO. This is further confirmed by the significnt decrease in the FTIR peks at 454, 668 and 803 cm^{-1}. The bright-field TEM (Fig. 1a) of TiO_2 indicated hollow box like structures with narrow size distribution and good morphological uniformity. The TiO_2 nanoboxes on graphene sheets (Fig. 1b) showed well dispersed NPs on both the graphene sides. The reduced graphene oxide is transparent with wrinkles and hollow TiO_2 structures (HRTEM, lattice spacing of 0.35 nm, Fig. 1c), confirming the (101) planes of the anatase TiO_2. The SAED pattern (Fig. 1d) revealed a [010]-axis orientation, and the lateral

Sample	τ_1 (ns)	τ_2 (ns)	τ_3 (ns)	I_1 (%)	I_2 (%)	I_3 (%)	I_1/I_2
TiO_2	0.1985	0.3937	2.29	54.38	43.86	1.763	1.23
TG	0.2069	0.3864	2.313	50.1	48.3	0.669	1.03

Table 1. Positron life time and relative intensities of the TiO_2 and TG sample

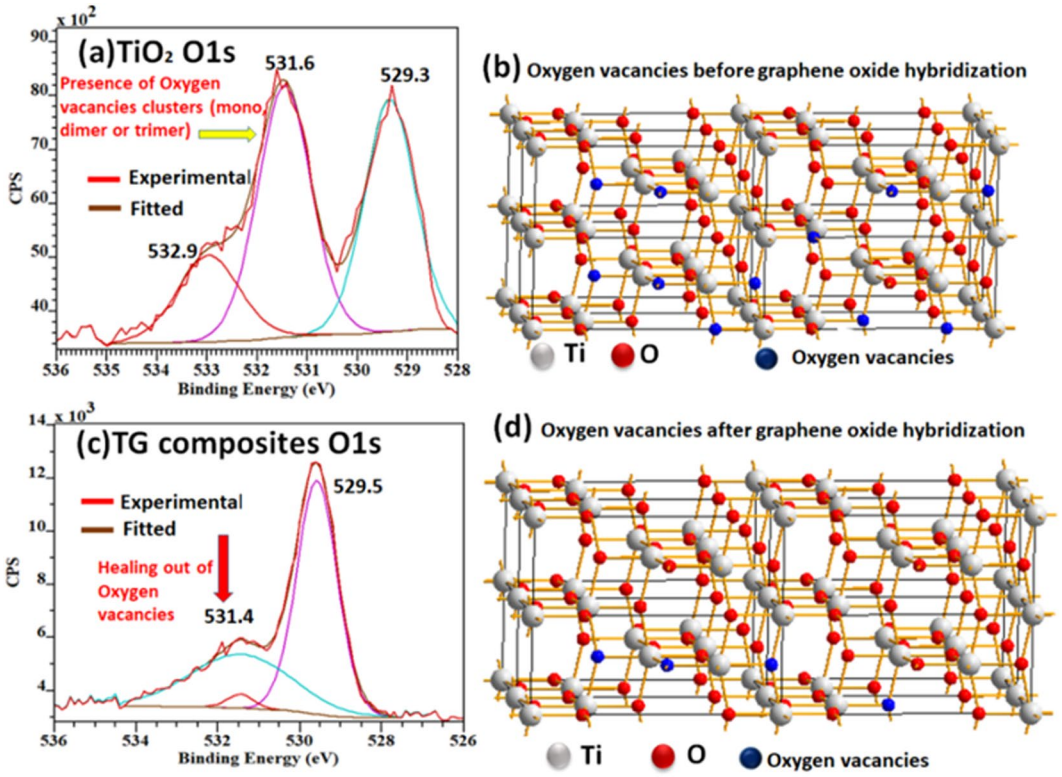

Figure 2. (**a**) XPS spectrum (TiO_2) of measured O1s spectrum, (**b**) simulated oxygen vacancies in 2*2-anatase crystal of the TiO_2 nanoboxes. (**c**) Measured XPS O1s spectrum of the TG composites. (**d**) Healing of the oxygen vacancies in the 2*2-anatase crystal.

plane of the of anatase corresponds to {010} facet that is vertical to the [010] orientation. The Fig. 1e STEM image shows hollow TiO_2 nanoboxes.

Defect characterization by PALS, XPS and EPR. Previous reports showed oxygen defects on the surface of TiO_2 raise the local-states under the edge of the conduction band. Oxygen defects densities with one or two electrons are generated due to the missing oxygen atom in the bulk or on the surface, while the Carbon doped TiO_2 forms deep impurity states in the band gap[1–3,10,11]. We observed (UV-vis spectrum, Supplementry Fig. 2) that bandgap of TiO_2 (3.2 eV) significantly decreased (2.6 eV) with increased absorption after hybridization with GO.

In this section, we used PALS (positron annihilation lifetime spectroscopy) to quantify the defect concentration obtained by the comparison of TiO_2 and TG composites. The Table 1 shows three positron lifetime components, τ_1, τ_2, and τ_3, with relative intensities I_1, I_2, and I_3 for the TiO_2 nanoboxes and TG composites. The shortest positron lifetime τ_1 (0.1985 ns) can be assigned to the bulk defects with free annihilation of positrons inside defect-free crystal[12]. Where as the longer lived positrons τ_2 (0.3937 ns) can be attributed to the surface defects originating from the positrons trapped by the larger defects such as oxygen vacancies or clusters, homodimers, trimers or larger[10]. The second positron lifetime components (τ_2) for the TiO_2 nanoboxes and TG composites are much higher than their respective first positron lifetime components (τ_1). The variation of τ_2 value from 0.3937 ns to 0.3864 ns was evident that the TiO_2 nanoboxes contain an abundance of surface oxygen defects and compressive bonding but reduced to atomic dimensions in the TG composites. The largest component (τ_3) is assigned to the micropores and to the annihilation of orthopositronium atoms[11]. Besides the lifetime factor of the positron, its relative intensity (I) gives information regarding the relative concentration of the defects[13]. The coupling of graphene oxide with TiO_2 leads to the decreased I_1/I_2 (1.23 to 1.03), thereby clearly indicates the relative bulk to surface defects concentration decrease.

The samples were further investigated by the XPS to get information about the chemical composition, oxygen vacancies and Ti oxidation-state inside TiO_2 nano-boxes after microwave treatment with the rGO. The O1s spectrum of TiO_2 nanobox (Fig. 2a) shows a peak at the binding energy of 529.3 eV, corresponding to the Ti(IV)

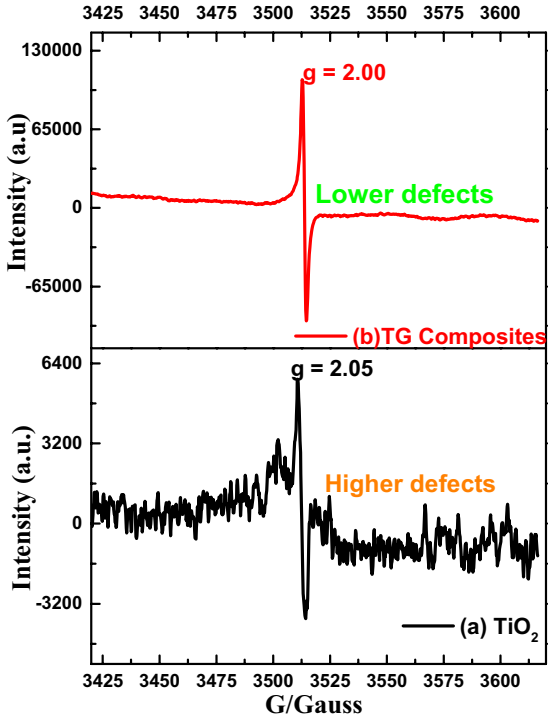

Figure 3. (**a**) EPR spectra of the TiO_2 and (**b**) TG composite at room temperature.

bound oxygen (O^{2-}). The peak at 531.6 eV can be attributed to the high binding energy component originated from the loss of oxygen (oxygen vacancies)[14]. The peak at 532.9 eV (low binding energy component), is due to the adsorption of HO^- on the surface. The O1s spectrum of TG composite (Fig. 2c) showed a strong O^{2-} peak at 529.5 eV. The second peak related to the oxygen vacancies O* (531.6 eV), showed significant suppression after rGO hybridization (microwave treatment). A slight shift (0.2 eV) in the peak position (529.5 eV) for the oxygen anions (Ti–O–Ti) is consistent with the Ti 2p core-level due to hybridization with graphene. Furthermore, inside TG sample the third low energy peak (near 532.9 eV) related to the surface hydroxyl group almost vanished. These observations confirmed that the concentration of surface defects is related with both surface hydroxyl groups and oxygen vacancies were significantly lowered in the hybrid sample[15]. The Fig. 2b,d schematically illustrates oxygen vacancies before and after GO hybridization.

The defects were further analyzed by the EPR (Fig. 3) because of the sensitivity of EPR towards the different defects, caused by the lower or extra electrons present on different atoms (O^-, O^{2-}, Ti^{3+}, Ti^{4+}) under different surrounding atoms (spin Hamiltonian, perturbation theory). The EPR spectra for the TiO_2 shows several peaks beside the main peak ($g = 2.05$). This observation clearly indicates presence of several types of defects. The previously reported EPR spectra indicated that the initial hole-trapper at the lattice of oxide ions at hydrated TiO_2 surfaces are the hydroxyl radicals. These trapped holes are the defect centers termed as bridging O^- species[16]. The presence of signal at $g = 2.05$ with broad underline peak in TiO_2 nanobox (Fig. 3a) represents the existence of significant oxygen vacancies[17]. This occurs because electrons trapped at Ti^{4+} sites can form Ti^{3+} (XPS, Fig. 2) and holes at subsurface oxide ions can form O^-[18]. The obtained EPR spectrum for the TG composites (Fig. 3b) shows a strong paramagnetic signal at $g = 2.00$ with loss of extra sharp-peaks. This represents the healing of oxygen vacancies (smoother spectrum) and other defects. Therefore we concluded that rGO hybridization has remarkably lowered the oxygen vacancies and other defects. These observations were further tested by the hydrofluoric acid (HF) addition experiments. Defects were introduced into TiO_2 by changing the amount of HF (details in Supplementary Information D2). The comparison showed defect introduction by the HF (0, 50 µL) changed the shape of EPR, introduced extra peaks (less smooth EPR) and modified the g value of TiO_2.

Absorption. The UV-Vis spectra of TiO_2 nano-boxes and composites (Supplementary Fig. 2) exhibit extended absorption therefore indicates lowered band gap of composites when compared with the standard TiO_2. The decrease in band gap has been attributed to the formation of C-Ti bond[19]. It is well-known that the extended absorption of light for the TG composite opens the possibility of higher photo-catalytic activity of a given photo-chemical reaction. Furthermore, considering the practical applications, the recyclability of photo-catalyst is another challenge to avoid contamination and higher economic efficiency. The photo-catalyst composites containing magnetite can easily separate from the solution by an external magnet. Therefore, the designing of efficient, magnetic photo-catalytic composite with reliable and stable structure has high importance. The non-toxic SiO_2 coating layer, conjugates well with functional groups, and known to protect Fe_3O_4 from oxidation thereby increases stability of NP-decorated photo-catalyst. Therefore, we have incorporated these materials to construct our photo-catalysts (TiO_2-Fe_3O_4@SiO_2)@graphene TFSG composite. The percentage of nanocomposites was TiO_2

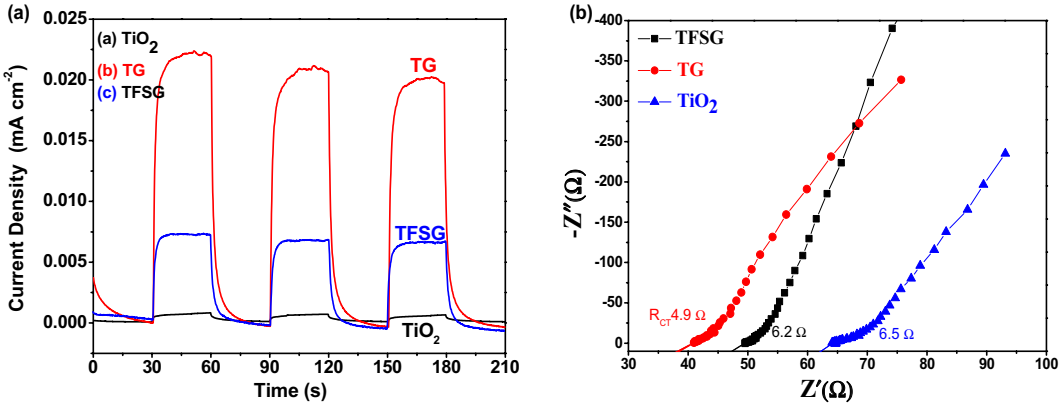

Figure 4. (**a**) I–t curves for the photocurrent responses of the TiO_2 nanoboxes (a), TG (b) and TFSG composites (c). (**b**) The Nyquist plot for the TiO_2 nanoboxes (a), TG (b) and TFSG composites (c).

(85%), Fe_3O_4@SiO_2(5%) and graphene (10%). The XRD spectra of TiO_2, Fe_3O_4@SiO_2 and (TiO_2-Fe_3O_4@SiO_2)@ graphene TFSG composite (Supplementary Fig. 3) indicates that all the samples are crystalline in nature. The obtained TFSG sample showed both peaks of TiO_2 and Fe_3O_4@SiO_2 nanoparticles (Supplementary Fig. 3(iii)), thus confirming the composite nature. The HRTEM of composites showed uniformely coated Fe_3O_4 with SiO_2 and and TiO_2 (Supplementary Fig. 4a,b).

The comparison of magnetic hysteresis loops related to the Fe_3O_4, Fe_3O_4@SiO_2 and TFSG composites (Supplementary Fig. 5) showed room-temperature ferromagnetism for the Fe_3O_4 and Fe_3O_4@SiO_2 and TFSG composites. The results show that there is a decrease in the magnetic saturation of TFSG composite due to the non-magnetic TiO_2. The saturation magnetization value (M_s) of the TFSG composites is 3.18 emu g^{-1}, which is lower than those of the Fe_3O_4@SiO_2 (57.48 emu. g^{-1}) and Fe_3O_4 (64.03 emu. g^{-1}). This value of magnetization is good for the efficient recovery of photo-catalyst.

Photocurrent and charge separation. The transient photocurrent response for the TiO_2, TG and TFSG composites were compared (Fig. 4a). The photocurrent (photo-electrochemical) response of the TiO_2 nanobox was weak (8.2×10^{-5} mA.cm^{-2}). While the TG composite showed significantly increased photocurrent response 2.344×10^{-2} mA.cm^{-2} (28.6 times higher) and 9.786×10^{-4} mA.cm^{-2} for the TFSG composites (11.96 times higher). This significant photo-current enhancement attributed to the lower recombination rate of electron–hole pairs and longer lifetime due to the presence of rGO sheets (2D π-π conjugation structure) as compared to the TiO_2. The comparison of EIS curves (Fig. 4b) showed the single-semicircles (Nyquist plots) in the high frequency range and a linear behavior in the low frequency region. The lowest charge transfer resistance (R_{ct}) was observed (4.9 Ω) for the TG composite when compared to the TFSG (6.2 Ω), and TiO_2 (6.5 Ω). Therefore, the TG composite exhibits the lowest R_{ct}, indicating lower charge-transfer resistance resulting in much faster separation of photo-generated species[20,21].

To verify the carbon detected in CO_2 conversion originates from the decomposition of photo-catalyst or from the added CO_2 gas, we carried out isotopic experiments by using traceable $^{13}CO_2$ under identical photo-catalytic reaction conditions. The products of photo-catalytic reaction were identified and quantified by the GC-MS (Supplementary Fig. 7). The ^{13}C, ^{13}CH, $^{13}CH_2$, $^{13}CH_3$ and $^{13}CH_4$ molecular fragments were detected. These observations from MS spectrum confirmed that the produced CH_4 indeed originated-from the reduction of CO_2 gas and not from the photocatalyst decomposition.

Photo-catalytic activities. The photo-catalytic activities of TiO_2 nanoboxes, TG composites and TFSG composites samples were evaluated for CO_2 conversion with triethanol amine as the electrons donor (Fig. 5a). The TiO_2 nanoboxes showed weak response for the photo-catalytic CO_2 conversion to CH_4 (~15.0 µmol g^{-1} h^{-1}) after 1 h irradiation. The TG composites demonstrate the highest (~49.0 µmol g^{-1} h^{-1}) activity for CO_2 conversion. Since, the TFSG composites were hybridized with magnetic nanoparticles (Fe_3O_4@SiO_2) for easier recovery thereby it showed lower CO_2 conversion to CH_4 activity (27.0 µmol g^{-1} h^{-1}) than TG, but still 3.2 times higher than that of TiO_2 nanoboxes (15.0 µmol g^{-1} h^{-1}). The main detected gas products were CH_4, H_2 and CO (GC analysis). The Fig. 5b shows the quantitative comparison of produced H_2 during this experiment. We further performed blank tests to confirm that CH_4 comes from the reduction of CO_2. After blank photo-catalytic experiment without CO_2 under the same conditions, we have not detected any CH_4.

The Fig. 6 shows comparison of time dependent H_2 evolution for the TiO_2, TG and TFSG composites. This water splitting reaction showed a sustained H_2 release rate of ~18.46 µmol/h for the TG composites. The standard solar light illumination for 8 hours, the hydrogen evolution kept increasing, demonstrating the robust photo-catalytic performance. This observation indicates stable and active photo-catalyst for long term water splitting. After conversion of CO_2 to CH_4 (5 h), samples were collected, washed several times and dried. The TEM results (Details in Supplementary information D3) showed stable composite after 5 h light irradiation.

The rate of H_2 evolution followed the following order: TG composites > TFSG composites > TiO_2 nano-boxes respectively. Quantum efficacies of these samples were calculated (Supplementary information 8) as 3.02%,

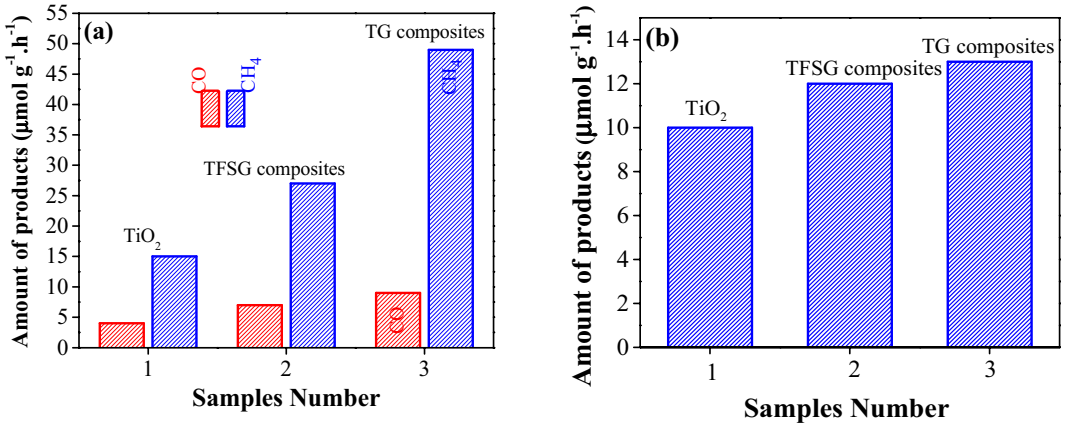

Figure 5. (**a**) Photocatalytic conversion of CO_2 to CH_4 after 1 h, (**b**) H_2 production by the photocatalysis (UV-Vis irradiation) of TiO_2 nanoboxes, TG composites and TFSG composites.

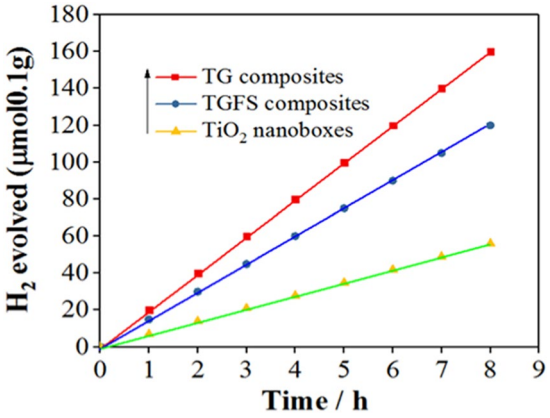

Figure 6. Time courses of H_2 evolution resulting from the reaction of water by TiO_2 nanoboxes, TG composites and TFSG composites irradiated with UV-visible light.

2.01%, and 0.3%, respectively for the TG, TFSG, and TiO_2 nanobox. In the CO_2 reduction, the photo-generated electrons-holes would migrate to the rGO surface. The conduction band of TiO_2 nano-boxes and the work function of rGO are reported as −4.2 eV and −4.42 eV, respectively[22,23]. The proximity of energy levels is helpful for the photo-generated species transfer from the TiO_2 nano-boxes conduction band to the rGO thereby produces radicals. The reason behind is the adsorption kinetics of the CO_2 (10^{-8} to 10^{-3} s) on TiO_2 nanoboxes is slower than the e-h recombination time (10^{-9} s)[24,25]. The composites increased the lifetime of the charged species that further improved the selective formation of CH_4 gas along with other minor product gases. The photo-catalytic performance supports our proposed interpretations of the CO_2 conversion to CH_4 through reduction mechanism.

As reported the hydroxyl radicals (·OH) are recognized to be important intermediates for CH_4 conversion. The mechanism of charge separation, coumarin fluorescence method (coumarin + •OH → fluorescent 7-hydroxycoumarin) is used to detect the amount of hydroxyl radicals (•OH) produced via photochemistry. The procedure relies on the basic principle that: the stronger the fluorescence signal being observed, the larger the •OH produced. We further compared the produced •OH for TiO_2 nanoboxes, TFSG and TG composites. The amount of produced •OH in TG and TFSG is larger than the TiO_2 nanoboxes (Fig. 7), with TG composites showing the highest fluorescence intensity. Hence, the TG composites produced highest amount of •OH thereby confirming the excellent photo-electrochemical and photo-catalytic properties.

In summary, we have explored the photo-catalytic reduction of CO_2 on TiO_2 nano-boxes, TiO_2 hybridzed with graphene (TG) and TiO_2-(Fe_3O_4@SiO_2)-rGO nanocomposite (TFSG). Oxygen clusters along with surface/bulk defects in TiO_2 nanoboxes play vital role in efficient photocatalysis. Positron annihilation results revealed decreased Oxygen clusters (mono, dimers, trimers) and the relative concentration ratio of bulk/surface defects in TiO_2 nanoboxes efficiently enhanced the photocatalytic mechanism. The photo-catalytic experiments and traceable isotopes containing carbon dioxide ($^{13}CO_2$) analyzed through mass spectroscopy confirmed the source of CH_4 production. The TG composite exhibits 3.2 times (~49.0 μmol g^{-1} h^{-1}) higher photo-catalytic reduction of CO_2 to CH_4, when compared to the TiO_2 nanoboxes. The TFSG composites retained magnetization, therby provides an easy way for the catalyst recyclability. The XPS study revealed that number of oxygen vacancies significantly decreased after GO hybridization, further confirmed by the EPR result. The excellent electrochemical and photo-catalytic properties were assigned to the lowered defects, proximity of energy levels, much higher

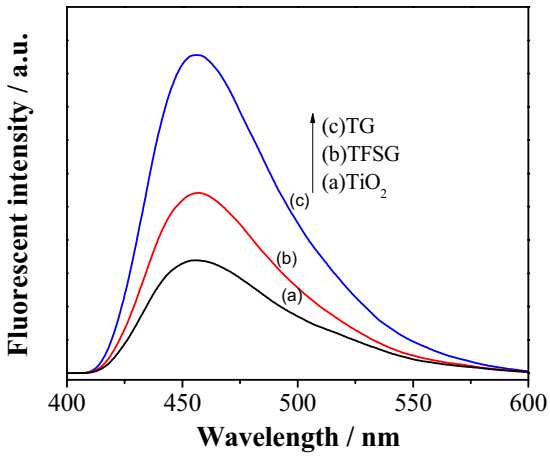

Figure 7. The •OH radical amount-related fluorescence spectra of (**a**) TiO_2 nanoboxes, (**b**) TFSG and (c). TG composites.

photo-current and higher quantum efficiency (3.17% @400 nm). We have presented 4 important evidences (positron annihilation (I_1/I_2 lowered), XPS (peaks 532, 531 eV decreased), EPR (smoothed, enhanced-signals), EIS (lowered charge-transfer resistance R_{CT}) confirming that the GO modified the TiO_2 to get appropriate photo-catalytic properties. Further by comparison and appreciation with the recent research[26–31] we believe, this research highlights the importance of meticulous design of the photo-catalysts required to improve the selective conversion of CO_2 towards valuable fuels[32].

Data Availability

The data sets generated during and/or analysed during the current study are available from the corresponding authors on reasonable request.

References

1. Leung, J. J. *et al*. Solar-driven reduction of aqueous CO_2 with a cobalt bis(terpyridine)-based photocathode. *Nat. Catal.* **2**, 354–365 (2019).
2. Wang, S. *et al*. Porous hypercrosslinked polymer-TiO_2-graphene composite photocatalysts for visible-light-driven CO_2 conversion. *Nat. Comm.* **10**, 676 (2019).
3. Zhang, Z. *et al*. Unraveling the Diffusion of Bulk Ti Interstitials in Rutile TiO_2 (110) by Monitoring Their Reaction with O Adatoms. *J. Phys. Chem. C* **114**, 3059–3062 (2010).
4. Berger, T. *et al*. Light-Induced Charge Separation in Anatase TiO_2 Particles. *J. Phys. Chem. B* **109**, 6061–6068 (2005).
5. Wang, X. *et al*. Trap states and carrier dynamics of TiO_2 studied by photoluminescence spectroscopy under weak excitation condition. *Phys. Chem. Chem. Phys.* **12**, 7083–7090 (2010).
6. Georgakilas, V. *et al*. Functionalization of graphene: covalent and non-covalent approaches, derivatives and applications. *Chem. Rev.* **112**, 6156–6214 (2012).
7. Zhang, H. *et al*. A facile one-step synthesis of TiO_2/graphene composites for photodegradation of methyl orange. *Nano Res.* **4**, 274–283 (2011).
8. Fu, Y. & Wang, X. Magnetically separable $ZnFe_2O_4$–graphene catalyst and its high photocatalytic performance under visible light irradiation. *Ind. Eng. Chem. Res.* **50**, 7210–7218 (2011).
9. Ricci, P. C. *et al*. Anatase-to-rutile phase transition in TiO_2 nanoparticles irradiated by visible light. *J. Phys. Chem. C* **117**, 7850–7857 (2013).
10. Liu, X. *et al*. Oxygen vacancy clusters promoting reducibility and activity of ceria nanorods. *J. Am. Chem. Soc.* **131**, 3140–3141 (2009).
11. Chakraverty, S., Mitra, S., Mandal, K., Nambissan, P. M. G. & Chattopadhyay, S. Positron annihilation studies of some anomalous features of Ni Fe_2O_4 nanocrystals grown in SiO_2. *Phys. Rev. B* **71**, 024115 (2005).
12. De la Cruz, R. M. *et al*. Effect of thermochemical reduction on the electrical, optical-absorption, and positron-annihilation characteristics of ZnO crystals. *Phys. Rev. B* **45**, 6581–6586 (1992).
13. Kong, M. *et al*. Tuning the relative concentration ratio of bulk defects to surface defects in TiO_2 nanocrystals leads to high photocatalytic efficiency. *J. Am. Chem. Soc.* **133**, 16414–16417 (2011).
14. Naeem, M. *et al*. Effect of reducing atmosphere on the magnetism of $Zn_{1-x}Co_xO$ nanoparticles. *Nanotechnology* **17**, 2675 (2006).
15. Pashandi, Z. *et al*. Photoinactivation related dynamics of ctenophore photoproteins: Insights from molecular dynamics simulation under electric-field. *Biochem. Biophys. Res. Commun.* **490**, 265–270 (2017).
16. Fujishima, A. *et al*. Biochemical application of photoelectrochemistry: photokilling of malignant cells with TiO_2 powder. *Electrochim. Acta* **38**, 153–157 (1993).
17. Susann, N. *et al*. Highly efficient rutile TiO_2 photocatalysts with single Cu(II) and Fe(III) surface catalytic sites. *J. Mater. Chem. A* **4**, 3127–3138 (2016).
18. Qiu, B. *et al*. Facile synthesis of the Ti^{3+} self-doped TiO_2-graphene nanosheet composites with enhanced photocatalysis. *Scientific reports* **5**, 8591 (2015).
19. Zhang, H., Lv, X., Li, Y., Wang, Y. & Li, J. P25-graphene composite as a high performance photocatalyst. *ACS nano* **4**, 380–386 (2009).
20. Cao, H. *et al*. Synthesis and superior anode performance of TiO_2@ reduced graphene oxide nanocomposites for lithium ion batteries. *J. Mater. Chem.* **22**, 9759–9766 (2012).
21. Wang, J. *et al*. Synthesis of hydrogenated TiO_2–reduced-graphene oxide nanocomposites and their application in high rate lithium ion batteries. *J. Mater. Chem. A* **2**, 9150–9155 (2014).
22. Zhu, G., Pan, L., Xu, T., Zhao, Q. & Sun, Z. Cascade structure of TiO_2/ZnO/CdS film for quantum dot sensitized solar cells. *J. Alloys Compd.* **50**, 7814–7818 (2011).

23. Yang, N., Zhai, J., Wang, D., Chen, Y. & Jiang, L. Two-dimensional graphene bridges enhanced photoinduced charge transport in dye-sensitized solar cells. *ACS nano* **4**, 887–894 (2010).
24. Woan, K., Pyrgiotakis, G. & Sigmund, W. Photocatalytic carbon-nanotube–TiO_2 composites. *Adv. Mater.* **21**, 2233–2239 (2009).
25. Hoffmann, M. R., Martin, S. T., Choi, W. & Bahnemann, D. W. Environmental applications of semiconductor photocatalysis. *Chem. Rev.* **95**, 69–96 (1995).
26. Cui, W. *et al.* Ba-vacancy induces semiconductor-like photocatalysis on insulator $BaSO_4$. *Applied Catalysis B: Environmental* **253**, 293–299 (2019).
27. Dong, X. *et al.* Promoting ring-opening efficiency for suppressing toxic intermediates during photocatalytic toluene degradation via surface oxygen vacancies. *Science Bulletin* **64**, 669–678 (2019).
28. Li, X. *et al.* Reactant activation and photocatalysis mechanisms on Bi-metal@ Bi_2GeO_5 with oxygen vacancies: A combined experimental and theoretical investigation. *Chemical Engineering J.* **370**, 1366–1375 (2019).
29. Li, J. *et al.* Probing ring-opening pathways for efficient photocatalytic toluene decomposition. *J. Mat. Chem. A* **7**, 3366–3374 (2019).
30. Huo, W. C. *et al.* Synthesis of Bi_2WO_6 with gradient oxygen vacancies for highly photocatalytic NO oxidation and mechanism study. *Chemical Engineering Journal* **361**, 129–138 (2019).
31. Huo, W. *et al.* Carbonate-intercalated defective bismuth tungstate for efficiently photocatalytic NO removal and promotion mechanism study. *Applied Catalysis B: Environmental* **254**, 206–213 (2019).
32. Humayun, M. *et al.* Enhanced visible-light activities of porous BiFeO3 by coupling with nanocrystalline TiO_2 and mechanism. *Appl. Catal. B: Environmental* **180**, 219–226 (2016).

Acknowledgements

This work is financially supported by the Fundamental Research Funds for the Central Universities (grant nos. 2015ZP024, 2015ZP030 and 2015ZZ063), Educational Commission of Guangdong Province (Grant No. 2014KZDXM010), National Natural Science Foundation of China (Grant No. 51774146), Guangzhou Municipal Science and Technology Program (Grant No. 201605120111410).

Author Contributions

Dr. G. Ahmed, Dr. F. Raziq, Dr. M. Hanif, Dr. J. Khan and Dr. K.S. Munawar participated in the experiments, figures, data explanations and manuscript writing other than PALS experiments. Prof. X. Cao did positron annihilation lifetime spectroscopy experiments (PALS) and provided related details. Prof. M.M. Wu and Prof. Z.W. Liu as the group leaders provided inspiration, helpful guidelines, refining of concepts and explanations.

Additional Information

Supplementary information accompanies this paper at https://doi.org/10.1038/s41598-019-49694-w.

Competing Interests: The authors declare no competing interests.

Publisher's note: Springer Nature remains neutral with regard to jurisdictional claims in published maps and institutional affiliations.